Transactions, SMiRT-25

Charlotte, NC, USA, August 4-9, 2019
Division II Fracture Mechanics and Structural Integrity

FRACTURE TOUGHNESS CHANGES WITH SURFACE CRACK DEPTH – THE "BACK-SURFACE" CONSTRAINT EFFECT

Gery Wilkowski, Suresh Kalyanam, Sushma Pothana, Yunior Hioe, Fabian Orth, Mo Uddin, Frederick Brust

Engineering Mechanics Corporation of Columbus, Columbus, OH, USA

ABSTRACT

Load-controlled leak-versus-break behavior observed from past circumferential surface-cracked pipe tests were poorly predicted from circumferential flawed pipe limit-load analyses. However, recent findings from surface-cracked pipe and SENT tests showed a toughness decrease with an increase in surface-flaw depth when looking at upper-shelf fracture behavior [Hioe *et al.* (2017)]. This demonstrated the significance of changes in the failure mode from limit-load to elastic-plastic fracture for deeper flaws where the toughness dropped significantly, even when considering materials where limit-load material behavior/condition was considered to exist. Hence, this explained some of the observations from past surface-cracked axial/circumferential pipe tests [Eiber *et al.* (1971)].

The flaw depth effect on toughness was observed in past experiments on surface-cracked flat plates. From these investigations, it was found that for surface-cracked axial pipe analysis the long-used semi-empirical surface-crack bulging factor (developed by Maxey/Kiefner), which is commonly employed in various international pipeline codes and standards, implicitly accounts for the toughness changes with flaw depth as well as the geometric effects of the bulging seen in axial surface cracked pipe experiments. The concomitant effect of the change in toughness with flaw depth is that highly conservative predictions will be made when assuming constant fracture toughness for a large range of surface-crack depths. A related paper [Kalyanam, Wilkowski *et al.* (2019)] in this SMiRT25 conference found that the toughness in a wrought TP304 circumferentially surface-cracked elbow at the start of ductile tearing was close to one-third of the fracture toughness determined from a Compact-Tension specimen test from the same material.

In addition to the cases of circumferential surface-cracked TP304 material in pipes and elbows, toughness decrease with increasing flaw depth was also observed for a large range of strain-hardening materials.

A three-dimensional elastic-plastic finite element (FE) analyses of the TP304 SENT specimens with three different initial crack depths (a_i/W) was conducted to determine the state of stresses ahead of the crack-tip that could shed light on the nature of constraint on the plastic zone developed and elastic-plastic J-values for ductile tearing. The FEA results of the three SENT specimens with initial flaw depths ranging from a_i/W=0.29 to 0.89 revealed that, although the toughness decreased by a factor of 5 ~ 6 over this range of flaw depths, the elastic-plastic constraint parameter, Q_i, at the start of ductile tearing was the same for all three SENT specimens over a range of distance ahead of the crack tip (normalized distances of $r\sigma_o/J$ from 0.25 to 1.5). In addition, it was found that the value of Q_i was more consistent at a distance of $r\sigma_o/J$=1.5 than the more commonly used $r\sigma_o/J$=2 in J-Q evaluations. An additional takeaway message was that using one SENT test result (one value of a_i/W), the fracture toughness, J_i at the start of ductile

tearing can be calculated. Although this was consistent with the experimental observations, the J_i for the different initial crack depth SENT specimens was not proportional to the Q-values at a given normalized distance ($r\sigma_o/J$) ahead of the crack tip, as is conventionally assumed.

INTRODUCTION

A constraint correction on the crack-driving force (i.e. normalizing the applied J-values by a Q-parameter value to account for different specimen geometries) has been employed in fracture toughness-based evaluations until date. The rationale being that the correction factor captures the constraint effects and allows for toughness data from a CT specimen to be used for prediction of behavior of other cracked pipe geometries. Hence, the methodology accounts for constraint on the crack-driving force calculations, while the toughness values are held as a constant. An alternate to this methodology is to employ calculated J or CTOD values and then apply a constraint correction factor on the material toughness. The experimental data trends lend themselves to empirical corrections on the material toughness. Also, the same experimental data can be employed to validate the constraint-adjusted crack-driving force approach.

While there are a host of constraint parameters (T-stress, J-Q, $\beta=T(\pi a)^{0.5}/K_I$, etc.) that explore elastic, and elastic-plastic material behaviour responses, it is important to classify them based on what they are able to capture as well as what is necessary for the structural assessment of pipe or other components [Hackett *et al.*(1991)]. The current investigation results explored the effects of constraint on upper-shelf fracture toughness for surface-cracked pipes and elbows. The applicability of the J-Q theory was assessed based on a selected set of experimental data and computational FE analyses. Past experience with US NRC related work has shown that the use of extrapolated CT J-R curves in the assessment of circumferential through-wall cracked pipes works well, which led to the formulation and use of Z-factors in Section XI of the ASME Boiler and Pressure Vessel Code [ASME BPVC (2016)]. Contrarily, the CT specimen J-R curves were never suitable in the prediction of surface-cracked pipe behaviour. Although, the CT specimen toughness has been considered and used as a lower bound toughness estimate in pipe and component flaw assessment, it has more recently been found that it may not be lower than the surface-cracked component toughness or toughness determined from SENT specimens [Kalyanam, Wilkowski *et al.* (2019)].

Detailed FEA provides a good evaluation of the crack driving force. Recent axial surface-crack analyses showed that when using a constant fracture toughness value leak-before-break (LBB) cannot be predicted, see Figure 1[Anderson (2014)]. However, many past axial surface-cracked pipe experiments shown in Figure 1[Eiber *et al.* (1971), *Maxey et al.* (1972)] indicate that LBB behavior does really occur. LBB is seen in Maxey empirical axial crack analyses and elsewhere in Section XI [ASME BPVC (2016)]. It is important to understand why there is a difference when examining past axial surface crack rupture experiments with newer FEA solutions. More importantly, the differences are notable with deeper surface cracks. Net-Section-Collapse (NSC) analysis for circumferential surface-cracks shows that surface-cracked pipe failure curves are always above the through-wall-cracked (TWC) pipe curves, so load-controlled leak behavior is not predicted (see Figure 2). Figure 3 shows an example from earlier work [Wilkowski and Eiber (1981)] for a circumferential surface-flawed pipe under bending loads in carbon steel materials with 4-inch and 30-inch OD pipes. Similar LBB behavior was also seen in the work of other researchers [Stadtmüller and Sturm (1995)] and is shown in Figure 4.

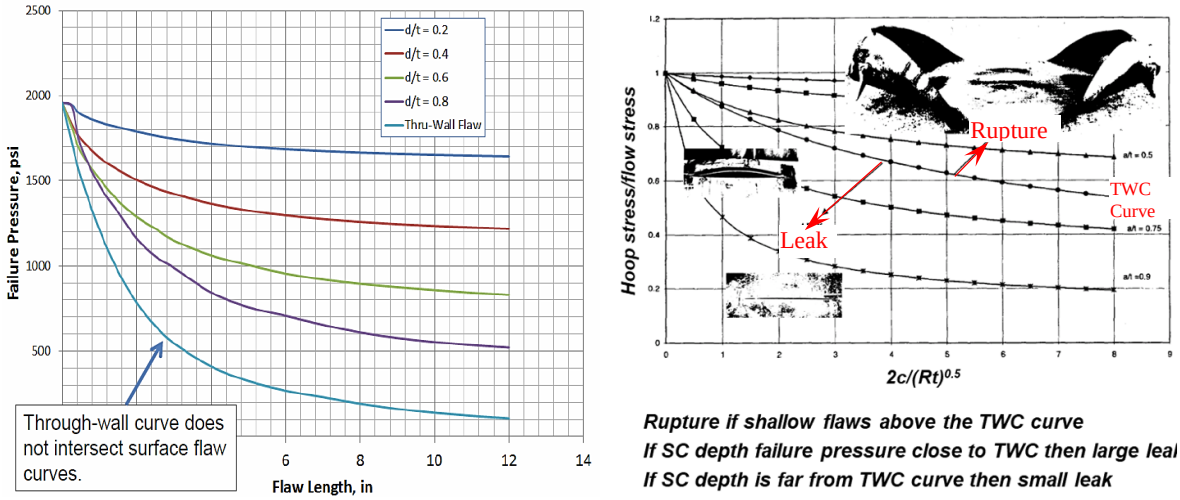

Figure 1. Results from FEA for axial surface-cracked pipes and through-wall-cracked pipes assuming the toughness is constant for all crack cases [adapted from Anderson (2014)] (Note, US units used in reference), and examples of leaks from axial-surface-cracked pipe tests, quick arrest due to rapid decompression, and rupture in nuclear piping at light water reactor (LWR) temperatures [adapted from Eiber et al. (1971)].

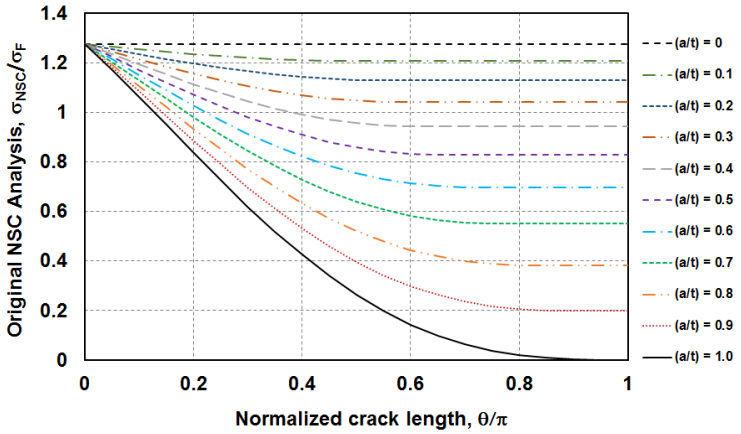

Figure 2. Original NSC analysis predictions for circumferentially surface-cracked pipe under pure bending [Kalyanam, Wilkowski *et al.* (2017)].

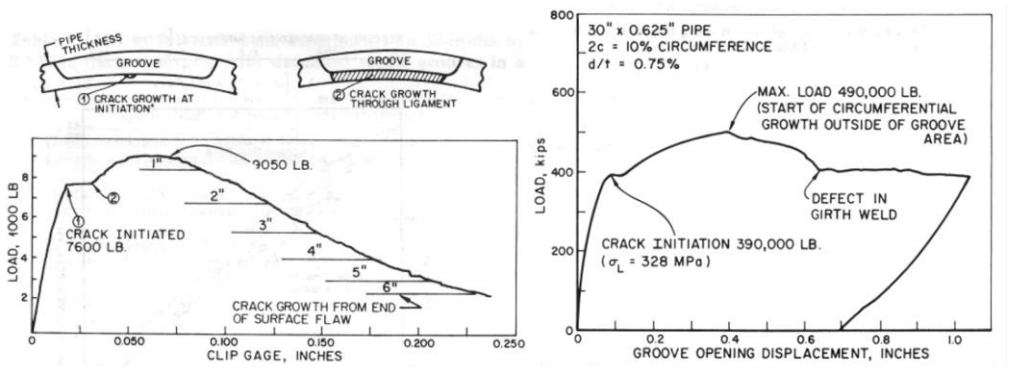

Figure 3. Examples from earlier data on circumferential surface-flawed pipe in bending showing LBB behavior [adapted from Wilkowski and Eiber (1981)].

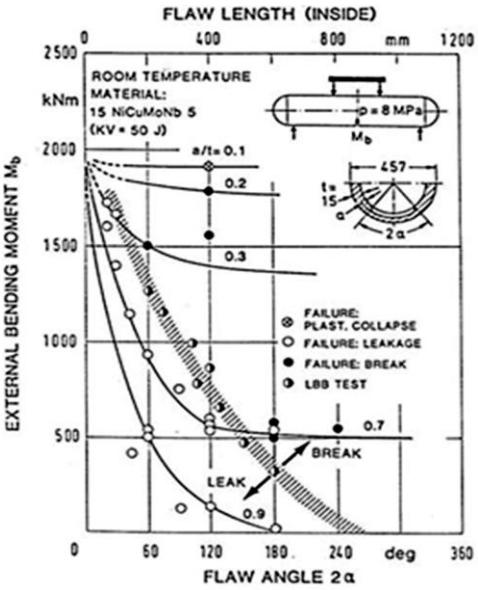

Figure 4. Experimental data on 18-inch (457-mm) outside diameter by 0.590-inch (15-mm) thick German alloy (15NiCuMoNb5) pipe showing lower maximum moments for deep surface cracked pipes compared to through-wall cracked pipes with crack lengths of the same length as the surface cracks [adapted from Stadtmüller and Sturm (1995)].

Toughness decreases with increasing flaw depths could explain the existence of load-controlled LBB for axial and circumferential surface-cracked pipes. Maxey's empirical axial surface-crack bulging factor that is in several international standards is inherently a combination of toughness change with flaw depth and the much smaller effect of bulging to predict LBB. The NSC limit-load for circumferential surface cracks does not predict load-controlled LBB, however surface-cracked pipe tests show that LBB occurs. This happens experimentally because the failure mode is changing from limit-load to EPFM failure as a/t increases (even in wrought TP304). The same kind of deep flaw LBB behavior has also been observed in flat plates. These behaviors spurred an interest in obtaining crack growth resistance (J-R) curves for various flaw depths in SENT (a/W) and surface-cracked pipes (a/t) experimentally. Recent work that explored the surface-cracked pipe fracture behaviour showed that the toughness decreased as the flaw depth to thickness ratio (a/t) increased. This work is ongoing at Emc^2 and is in the state of evolution towards development of empirical relations that can depict fracture toughness changes with crack depth. Figure 5 shows a popular ideology of a back-surface constraint effect that refers to the constraint from the back-surface restricting the amount of plasticity developed in the specimen, which is very different from the examination of the constraint effects using a near crack-tip constraint parameter.

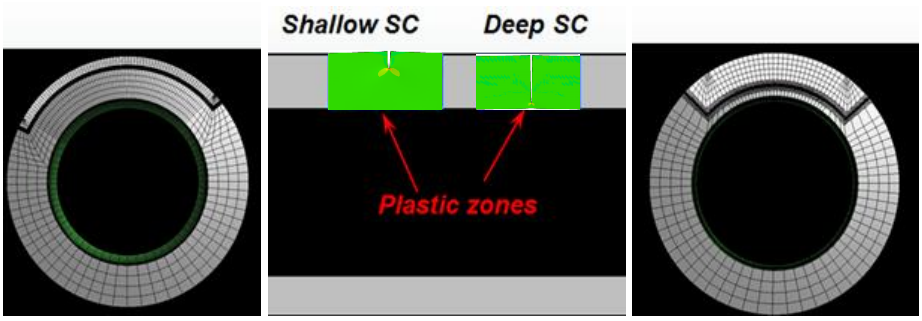

Figure 5. Back-surface constraint effect on plasticity – schematic.

In this paper, the data trends from several studies are examined, and then a J-Q analyses of one set of TP304 material SENT test data developed at room temperature are used to examine the normalized stresses ahead of the crack front, and the Q values for different SENT specimens with various a/W values. Elastic-plastic ABAQUS FE analyses were conducted up to the start of ductile tearing and the results were examined to arrive at stress distributions near the crack to see how Q might vary with a/W.

INITIATION TOUGHNESS CHANGE WITH CRACK DEPTH IN SENT, SC-PIPE, AND CT SPECIMENS

A linear trend in the crack-tip-opening displacement at crack initiation ($CTOD_i$) determined at 0.2mm of crack growth from unloading compliance data (near start of ductile tearing) was found with normalized initial crack depth (a_i/W) in X100 high-strength carbon steel SENT specimens (a_i/W=0.25, and 0.5) tested at room temperature [Park *et al.*(2010)]. A decrease in crack-initiation toughness with the increase in normalized crack depth, a_i/W was seen. Further, the extrapolated linear variation of $CTOD_i$ with a_i/W revealed that the value of $CTOD_i$=0 when the a_i/W=1 as shown in Figure 6, which is also shown as a normalized $CTOD_i/(W-a_i)$ variation with a_i/W of the SENT specimens in Figure 6.

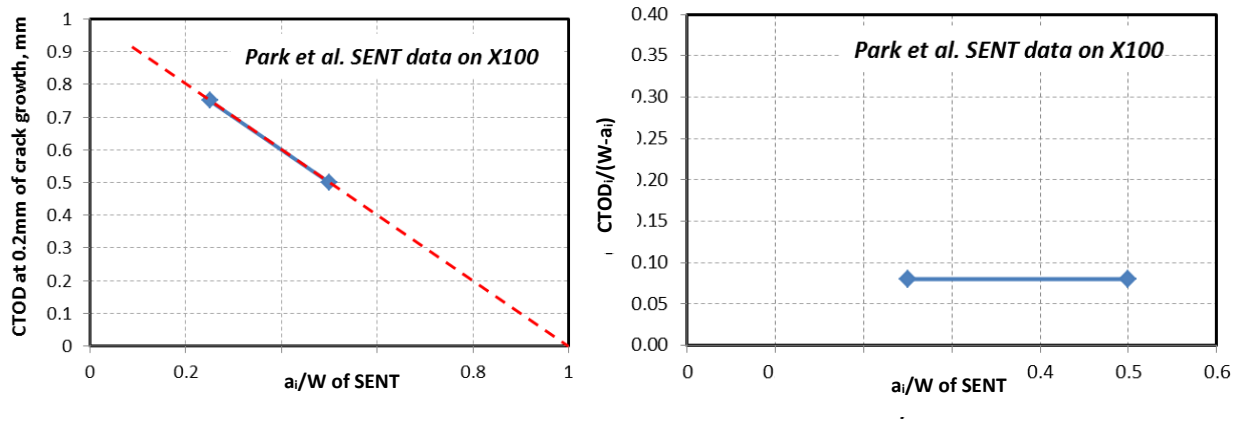

Figure 6. CTOD and normalized $CTOD_i/(W-a_i)$ variation with a/W for SENT specimens machined from X100 steel and tested at RT.

Experiments with TP304 SENT specimens (from 3-inch nominal diameter and Schedule 160 thickness) having four different normalized crack depths (a_i/W=0.3, 0.5, 0.7, 0.9) showed similar trends to those seen in the X100 steel [Hioe *et al.* (2017)]. The CTODs from the eight SENT tests were obtained using a double clip-gage technique [Kalyanam, Wilkowski, *et al.* (2010)] and the start of ductile tearing (crack initiation) determined using a d-c EP technique [Wilkowski and Maxey (1981)]. A linear trend of CTOD with crack depth, a_i/W was seen such that when extrapolated the CTOD=0 at a_i/W=1. Upon nondimensionalization of the CTOD using initial ligament length ($W-a_i$), Figure 7 shows a nearly constant value over the range of a_i/W of the SENT specimens. The crack initiation toughness change with crack depth was clearly evident.

The elastic–plastic fracture parameter, J_i [Rice (1968), Rice and Rosengren (1968)] was evaluated for the eight TP304 SENT specimens. Figure 8 shows a linear trend in the J_i (at crack initiation) that was found with the initial crack depth, a_i/W akin to the $CTOD_i$, and also demonstrates a decrease in toughness at the start of ductile tearing as the initial crack depth (a_i/W) is increased. The intercept for a_i/W=1 was not at J_i=0, and could be attributed to the η-factor used in J_D evaluation, with the η-factor having some error for deeper initial cracks ($a_i/W > 0.6$). Figure 8 also shows the change in material fracture resistance, J_D-R curves for three SENT specimens with different initial crack depth, with the lowest J_D-R curve exhibited by the deepest initial crack depth specimen, a_i/W=0.9.

An important finding was that the $CTOD_i$ variation with the initial crack depth, a_i/W was different for a surface-cracked pipe and a SENT specimen obtained from the same TP304 material and tested at RT. Figure 9 shows that the $CTOD_i$ at the start of ductile tearing (for SENT specimens with a_i/W= 0.3 ~ 0.9, SC pipe with a_i/W=0.4 ~ 0.8) was roughly four (4) times larger in the case of the pipe when compared to the SENT specimen demonstrating a difference in constraint between the two specimen geometries. Since this was a large difference between the SENT specimens and SC pipe, it is still under investigation through analytical and computational methods.

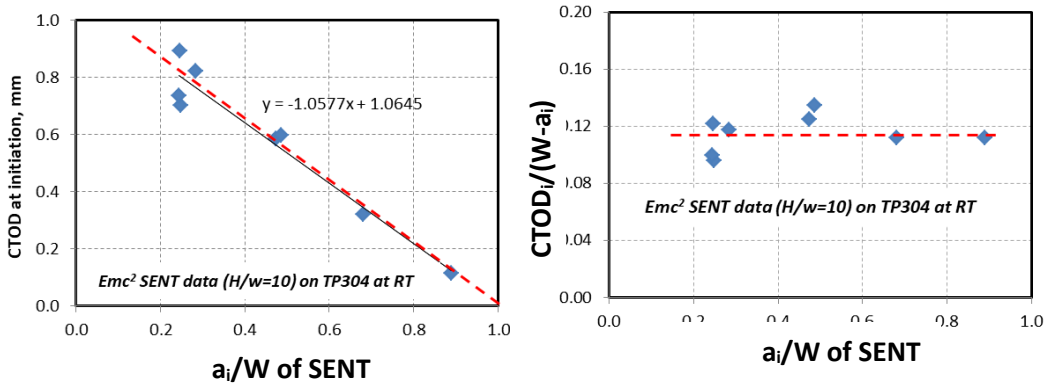

Figure 7. $CTOD_i$ and normalized $CTOD_i/(W-a_i)$ variation with a_i/W for SENT specimens machined from TP304 stainless steel and tested at RT.

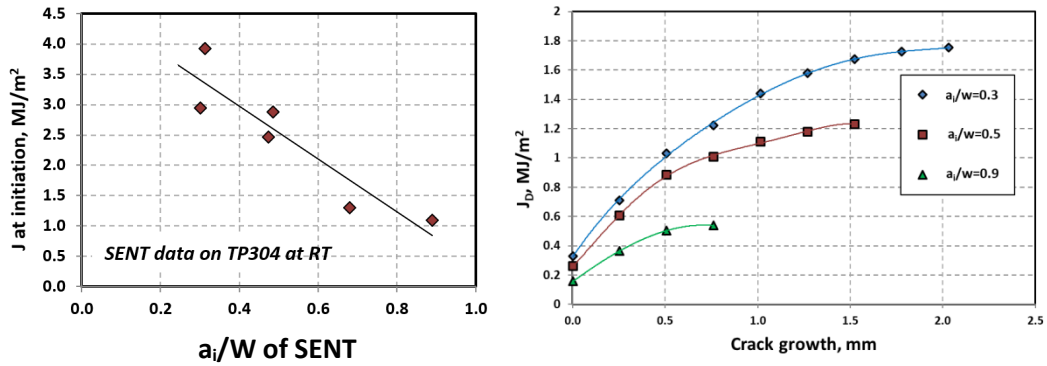

Figure 8. Variation of J_i (elastic-plastic fracture parameter J at crack-initiation) with a_i/W, and J-R curves (fracture toughness resistance curves) showing variation of J_D with crack growth, Δa for SENT specimens machined from TP304 stainless steel and tested at RT.

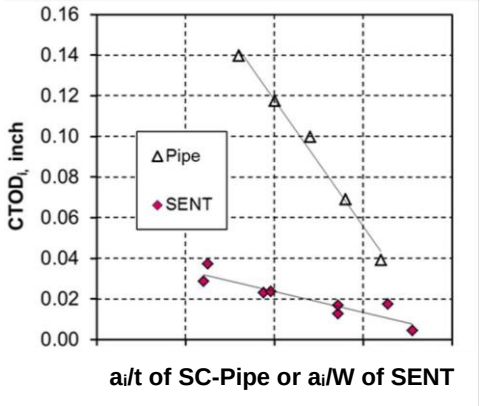

Figure 9. $CTOD_i$ (crack-tip-opening displacement at crack-initiation) variation with a_i/W for SENT specimens and with a/t for surface-cracked pipe – both from TP304 stainless steel material tested at RT.

An earlier International Piping Integrity Research Group-2 (IPIRG-2) experimental program was revisited where an elbow component and CT tests from the same material were conducted in the 1980s [Fleming *et al.* (1996) [1]]. A FEA model of the surface-crack profile in the ID of the elbow measured from post-test fractography and reported in the Elbow Experiment 2-4 Data Record Book [Fleming *et al.*(1996)[1]] was used to model the elbow experiment (see Figure 10). The FEA model of the IPIRG-2 Elbow Experiment 2-4 (comprised of A710 carbon steel pipes attached to TP304 elbow and tested at 550 F and 2,250 psi internal pressure) is shown in Figure 10. FEA was conducted to determine the initial crack depth, a_i/W for the duplicate SENT specimens tested at elevated temperature of 550 F (288 C) (corresponding to the peak elastic-plastic fracture toughness J value determined along the non-uniform crack front in the ID surface-cracked elbow). Details of the modeling and results from the elbow FEA are presented in a related paper in this SMiRT25 conference [Kalyanam, Wilkowski, *et al.* (2019)]. Figure 11 shows a comparison of the SENT, CT, and elbow component results. The crack-initiation fracture toughness, J_i was found to be about 2.2 ~ 2.9 times larger in the duplicate CT specimens tested (J_i=6.1 in-kip/in^2) [Fleming *et al.* (1996)[1]] when compared to the SENT and elbow specimens, which were closer. This demonstrated that the constraint in the SENT and SC-pipe (with comparable crack depth, *i.e.* $a_i/W=a_i/t=0.68$) were closer than the CT specimen ($a_i/W=0.5$).

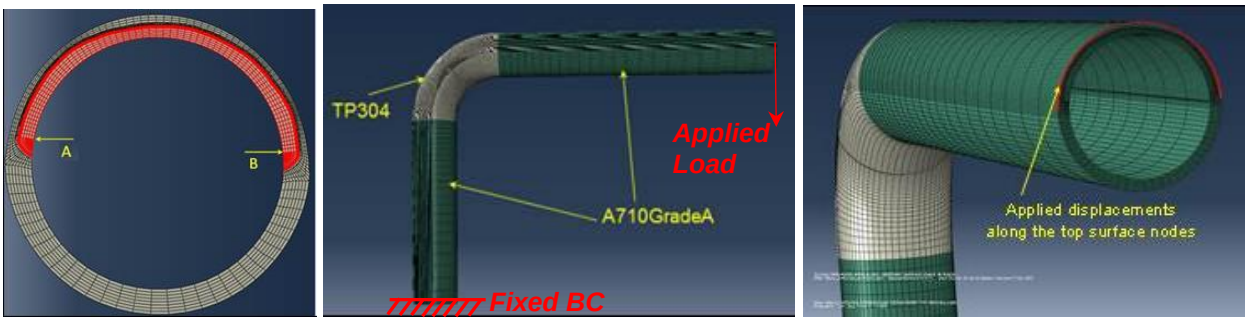

Figure 10. FE mesh created using PipeFracCAE© showing variation of the surface-crack depth (after fatigue precracking) along the 180-degree circumferential ID surface-crack length, and FE model of the elbow test frame used in the FE analyses with boundary conditions (BC) and the wire rope loads applied along the outer surface nodes in the FEA.

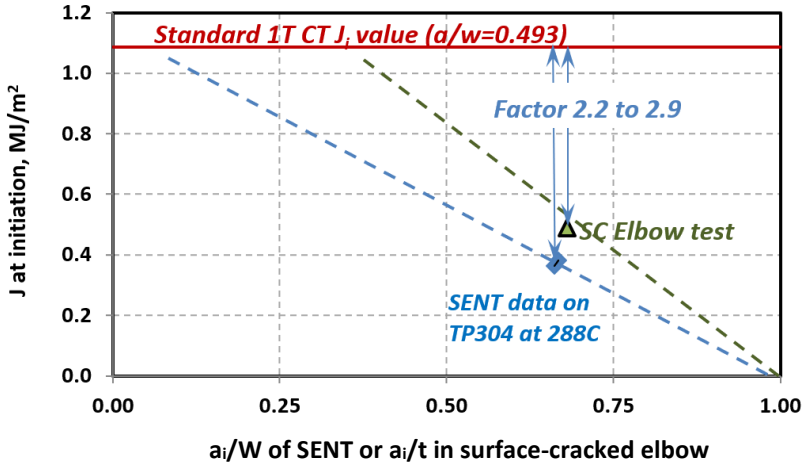

Figure 11. Elastic-plastic J-value at crack initiation, J_i from the CT, SENT, and the IPIRG2 surface-cracked Elbow Experiment 2-4.

[1] M. Fleming, T. Kilinski, P. Scott, G. Wilkowski, Data Record Book Entry E-2.2.2.1ic.2 for IPIRG-2 Experiment 2-4 in NUREG/CR-6444 BMI-2192, 1996.

Using a fourth set of data (X80 material from 36-inch diameter pipe [Shim, Wilkowski, *et al.* (2010)]) comparison of the initiation toughness in terms of $CTOD_i$ showed that the variation with a_i/W (or a_i/t) followed the same linear trend for the SENT and axial surface-cracked pipe ($CTOD_i$ decreased with increasing a_i/W or a_i/t and reached $CTOD_i=0$ at $a_i/t=1$ similar to those seen from circumferential surface-cracked pipes).

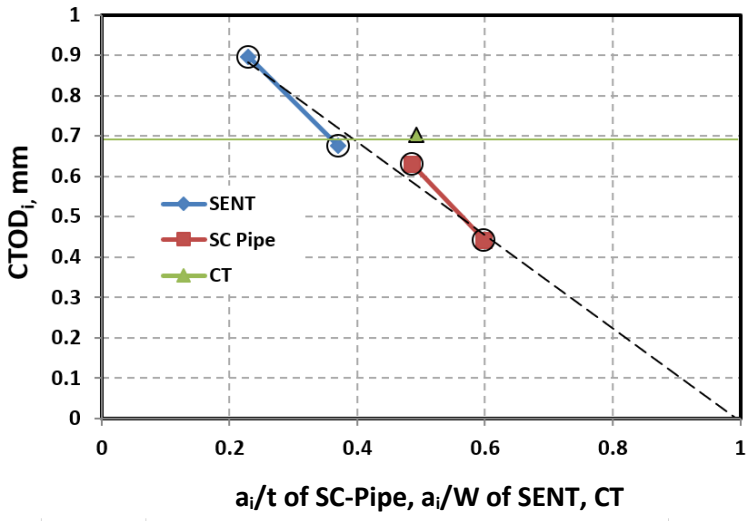

Figure 12. $CTOD_i$ variation with a_i/W for SENT specimens and with a_i/t for axial surface-cracked pipe – both from X80 line-pipe steel tested at room temperature.

A methodology, outlined in the schematic in Figure 13, can be established for the initiation toughness change with flaw depth through constraint corrections to determine the fracture toughness of surface-cracked pipe and SENT specimens using the ASTM standard CT specimen ($a_i/W=0.5$). The relationships would need to be established for variables governing each material, and test conditions.

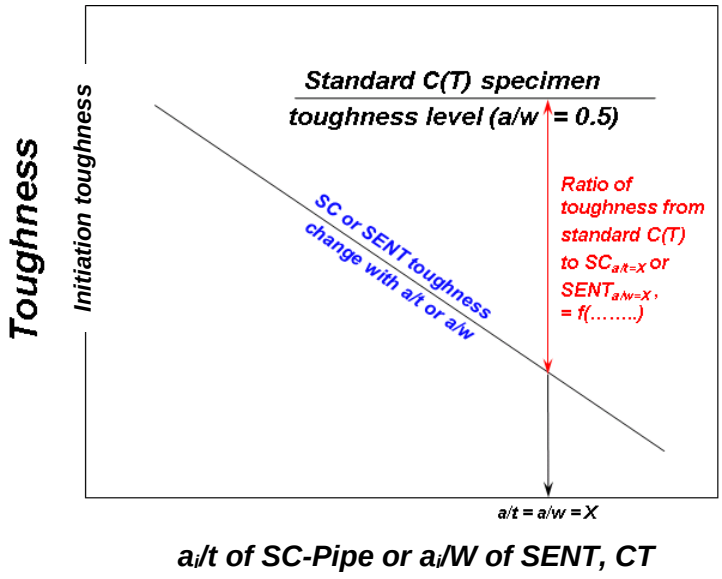

Figure 13. Schematic of possible toughness variation with a_i/t in surface-cracked pipe or a_i/W in SENT or CT specimens.

DOES J-Q THEORY ON CONSTRAINT CAPTURE THIS INITIATION TOUGHNESS TREND WITH THE FLAW DEPTH CHANGE IN SENT SPECIMENS?

A J-Q theory was developed by researchers in the 1980s to address the effect of constraint in elastic-plastic fracture in various specimen geometries. Small-scale-yielding (SSY) models [Roychowdhury and Dodds (2003,2005)] can be used as reference solutions, where a single fracture parameter (K, J, CTOD) dominance is assumed. A two-parameter J-Q theory [O'Dowd and Shih (1991-I, 1991-II), O'Dowd et al. (1995), Dodds (1994)] allows for analysis of elastic-plastic fracture when single fracture parameter (K, J, CTOD) are not able to describe the crack-tip stress fields, which is especially true when large plastic zones are formed in a cracked component and the plastic zone is no longer within a constrained zone for shallow cracks and/or large loads. Equations 1 and 2 provide two-parameter crack-tip stress field descriptions with Equation 2 providing the value of Q obtained by comparison to the reference stress solution (SSY model [Roychowdhury and Dodds (2003)], Hutchinson-Rice-Rosengren HRR solution for power-law hardening material [Hutchinson (1968)]). Q parameter quantifies the difference between the stress state ahead of the crack-tip in the component/structure and the reference (SSY or HRR) solutions. Several other constraint parameters are available in the literature, but J-Q was selected for our initial evaluations [O'Dowd (1995), Graba (2008)].

$$\sigma_{ij} = \sigma_{ij}^{r} + Q\,\sigma_{ij}\,\delta_{ij} \tag{1}$$

$$Q = [\sigma_{ij} - \sigma_{ij}^{r}]/\sigma_{o} \tag{2}$$

where, σ_{ij} is the stress in the case being evaluated, σ_{ij}^{r} is the reference stress from plane-strain SSY model, HRR solution, δ_{ij} is the Kronecker-delta tensor, Q is the constraint parameter, and σ_o is the yield stress or an appropriately chosen constant from a plastic stress-strain relation for power-law materials (Ramberg-Osgood relation).

Figure 14 shows an example of the TP304 SENT specimen (a_i/W=0.29) modeled, with the spider mesh size chosen in relation to the plastic-zone size (larger for the shallow-cracked SENT specimen) using the J_i values (shown in Figure 15) obtained at crack-initiation from SENT experiments using an η-factor analysis[2]. In this investigation three TP304 SENT specimens with different initial crack depths (a_i/W=0.29, 0.68, and 0.89) were modeled using continuum C3D8R elements in ABAQUS [commercial FEA software from Dassault Simulia] to capture the stress state at the beginning of ductile tearing (crack-initiation). The SENT specimen FEA model was loaded to the displacement corresponding to the crack-initiation event (start of ductile tearing) determined from each of the three SENT experiments.

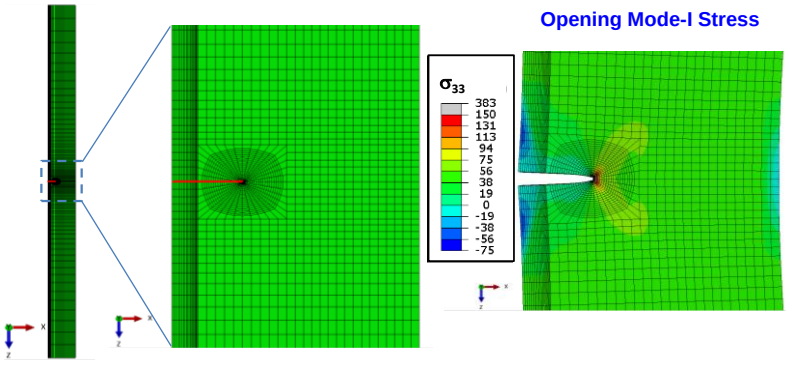

Figure 14. SENT specimen modeled with C3D8R continuum elements in ABAQUS with an elastic-plastic FEA mesh for a_i/W=0.29.

[2] η-factor is used as a plastic correction-factor that accounts for the geometry, specimen size, and loading method. η-factor used here was from the DNV-RP-F108 for a fixed-grip SENT specimen

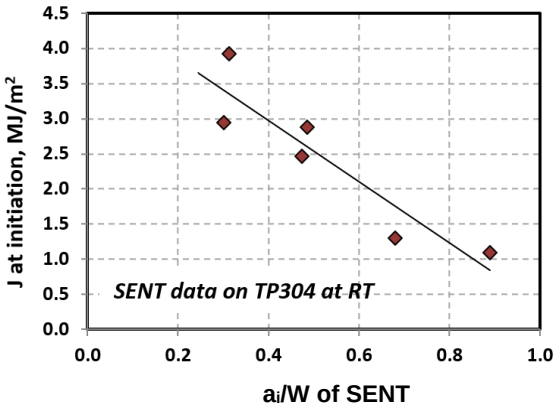

Figure 15. Variation of J_i with initial crack depth in SENT specimens from TP304 material tested at RT (J_i from η-factor analysis).

Figure 16 shows the SENT specimen mid-section with the crack opening at the start of ductile tearing and the crack opening-mode plastic strain, ε^p_{33} (ε^p_{33}= 0.25 chosen for the plastic-strain contour maximum based on the maximum value provided in the true-stress logarithmic strain input for FEA). Figure 17 shows the von-Mises stress at the start of ductile tearing for SENT specimen with a_i/W=0.29.

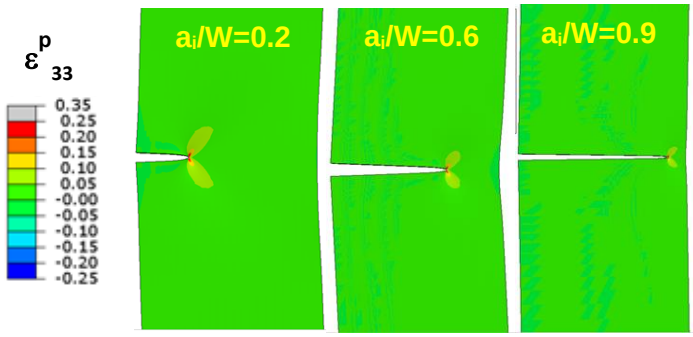

Figure 16. Mid-thickness of SENT specimen is shown with the crack-opening at the crack-initiation event and the opening-mode plastic strain (ε^p_{33} or PE_{33}) around the crack-tip in the SENT specimens modeled using FEA.

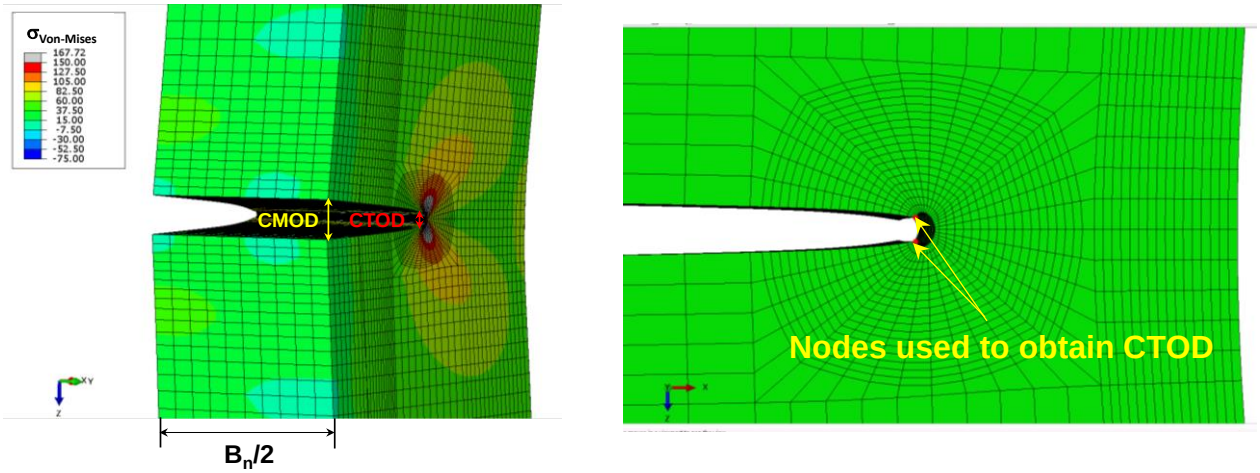

Figure 17. Mid-thickness of the SENT specimen is shown with the locations used to obtain the CMOD and $CTOD_i$ values from the FEA.

Figure 18 shows the opening-mode stress, σ_{33} in the three SENT specimens, indicating that most of the region ahead of the crack is yielding at the beginning of ductile tearing (yield stress, σ_o = 35.2 ksi). Opening–mode stress that is close to $3.7\sigma_o$ (innermost contour region/zone) is indicated in Figure 18 with the peak stress region being much smaller in the deeper notched SENT specimen at the beginning of ductile tearing. Peak stresses that are close to $3.7\sigma_o$ at a distance of $x=1\times\sigma_o/J$ from the crack-tip along the symmetry-plane (X-axis or $\theta=0$) was shown using large-strain numerical analysis [McMeeking and Parks (1979)]. Figure 19 shows the opening stress, σ_{33} through the thickness of the SENT specimens with crack depths of $a_i/W=0.29$ and $a_i/W=0.68$. Initially, the crack opening-mode stress, σ_{33} attained a peak value in the mid-thickness of the SENT specimen and dropped in value as the side-surfaces of the SENT specimen are approached. A second observation was that the stress contour regions proportionately scale with the depth of the crack in the SENT specimen, which can be correlated with the normalized opening stress variation with the distance ahead of the crack tip.

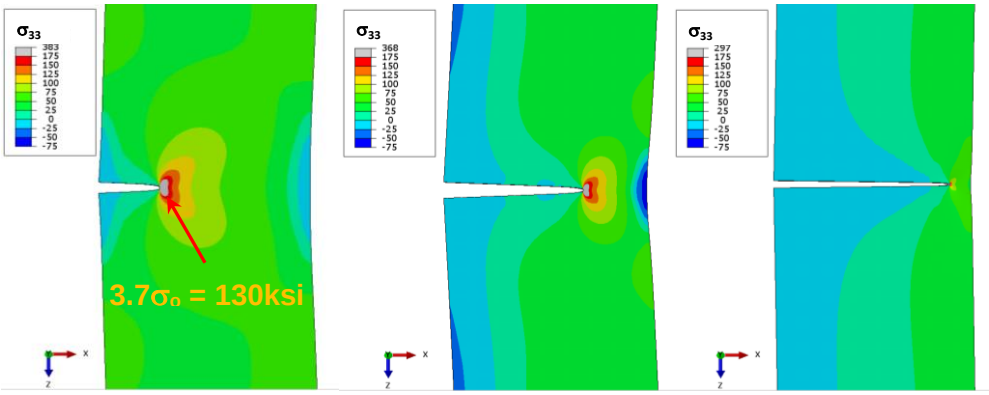

Figure 18. Opening-mode stress, σ_{33} contour seen in three SENT specimens at the crack-initiation event (identical stress color scales used in all three SENT specimens with $a_i/W=0.29,0.68, 0.89$).

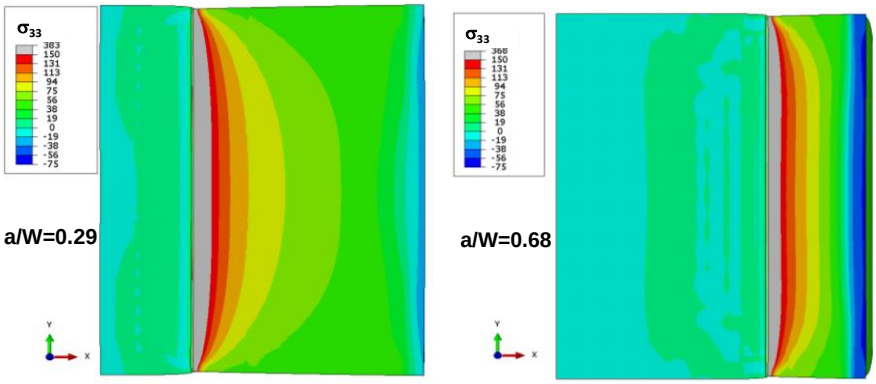

Figure 19. Opening-mode stress, σ_{33} contour seen through the thickness of SENT specimens with $a_i/W=0.29$ and 0.68.

Since the ligament length was smaller in the deep-cracked SENT specimens ($a_i/W=0.68$ and 0.89), when compared to the shallow-cracked SENT specimen ($a_i/W=0.29$), the crack opening-mode stress, σ_{33} ahead of the crack-tip obtained from FEA in Figure 20 spans a much smaller distance ahead of the crack-tip. Hence, after normalization (see Figure 20), where the opening-mode stress is scaled with distance expressed in a normalized fashion as $r\sigma_o/J$ (r is distance from crack-tip and J is EPFM parameter at the start of ductile tearing, and σ_o is the yield stress), they are all found to be self-similar in nature. To obtain a reference solution for comparison of the opening-mode stress field seen in the SENT specimens, a small-scale yielding (SSY) model with plane-strain constraint was used from a 3D non-linear FEA of

solids code [WARP3D]. This applied the same elastic-plastic material property used in the FEA of the SENT specimens, and hence provided a direct comparison between the SENT and reference SSY model [Roychowdhury and Dodds (2003), Kalyanam, Dodds *et al.*(2009), Sobotka and Dodds (2011)], without the use of power-law hardening model approximations such as a Ramberg-Osgood fit to the elastic-plastic material behavior employed in HRR solutions. Details of the SSY modeling and FEA results are presented elsewhere [Wilkowski, Kalyanam *et al.* (2019)].

Figure 21 shows a comparison of the reference plain-strain SSY model solution super-imposed on the SENT stress solutions. Although, a normalized distance of $r\sigma_o/J=2$ ahead of the crack-tip is commonly chosen for constraint characterization, observations from this work revealed that a closer match was found at a normalized distance of $r\sigma_o/J=1.5$, and was chosen for comparison [O'Dowd (1995), Graba (2008), Larossa and Ainsworth (2016)]. Further, it was observed that consistent normalized opening-mode stresses were seen at distances spanning $r\sigma_o/J = 0.25$ to 1.5 from the FEA results for the three SENT specimens, each obtained for the corresponding experimental load at the start of ductile tearing. Evaluation of the elastic-plastic constraint parameter, Q (difference between the SSY/Reference and SENT normalized opening-stress solutions) revealed that it has the closest match at a distance of $r\sigma_o/J_i=1.5$, but almost similar values over normalized distances of $0.25 < r\sigma_o/J_i < 1.5$. This led us to conclude that "***there exists a crack-tip constraint parameter, Q_i (or stress field condition) that is required to be reached for the crack-initiation event to occur in each of the SENT specimens***". However, caution needs to be exercised when applying this crack-initiation constraint condition or parameter, Q_i to a different specimen (CT, SENB) or pipe geometry (with axial or circumferential surface-crack). A different geometry dependent constraint parameter, Q_i^{CT}, Q_i^{SENB}, Q_i^{Pipe} may need to be reached for crack-initiation to occur in each of these CT, SENB, and SC-Pipe specimen geometries.

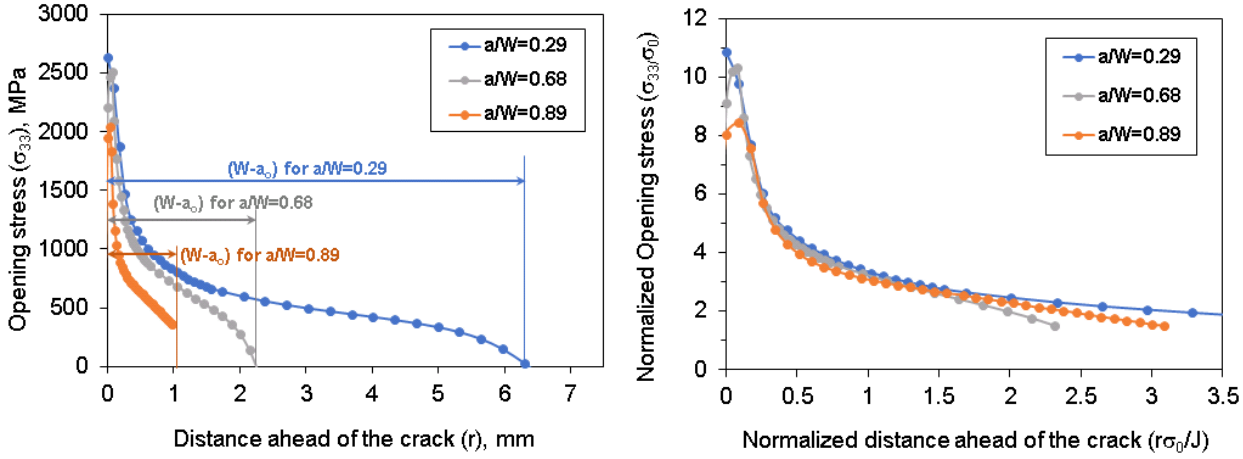

Figure 20. Opening-mode stress, σ_{33} variation with the distance from the crack-tip, r (in three SENT specimens with different initial crack depth, a_i/W); and normalized opening-mode stress, σ_{33}/σ_o variation with normalized distance from the crack-tip, $r\sigma_o/J_i$ determined at the experimental load corresponding to the start of ductile tearing in each SENT test.

The shallow-cracked SENT specimen ($a_i/W=0.29$) was revisited to capture the opening-mode stress fields at five different instances and to understand the change in crack-tip constraint parameter, Q starting from the applied loading and until the start of ductile tearing as observed during the SENT experiment when J_i= 0.248 mm-kN/mm^2 (1.415 inch-kip/inch^2). Figure 22 shows the opening-mode stress, σ_{33} obtained at five different applied displacement levels (corresponding J values at 0.067, 0.122, 0.165, 0.206, 0.248 mm-kN/mm^2), where the peak stresses were seen to increase as the displacement load/J-value increased. Upon normalization of the opening-mode stress (σ_{33}/σ_o) and showing the variation with normalized

distance ahead of the crack-tip ($r\sigma_o/J$), Figure 22 also shows the comparison to the normalized reference opening-mode stress (σ^r/σ_o) solution computed for the start of ductile tearing. The magnitude of Q was seen to increase with the applied loading until it reaches a value of Q_i corresponding to the start of ductile tearing. This demonstrates that the constraint changes as the plasticity develops around the crack-tip. Table 1 shows the applied displacement load, J-value, and Q-value comparisons obtained at the normalized distances of $r\sigma_o/J$ = 1.5 and 2.

The following Table 1 provides the applied remote displacement, elastic-plastic fracture parameter, J, and the Q-values obtained at the normalized distances, $r\sigma_o/J$ = 1.5 and 2 for the simulated SENT specimen with a_i/W=0.29 until the initiation toughness. Similarly, Figure 23 shows the change in Q starting from one-fifth of the experimental displacement at the start of ductile tearing (Disp. = 0.44 mm) in the SENT specimen until the crack-initiation event (Disp. = 2.03 mm). The Q-values were found to decrease with the increasing applied load on the SENT specimen, demonstrating a decrease in constraint as the load increased (applied displacement, J-values) and the plasticity around the crack-tip increased.

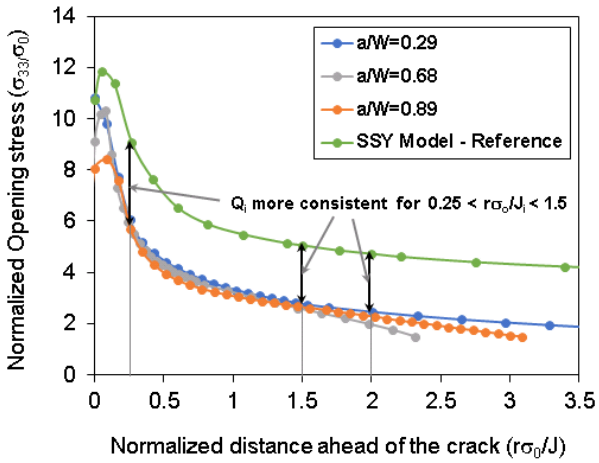

Figure 21. Normalized opening mode stress, σ_{33}/σ_o (three SENT specimens with different initial crack depth, a_i/W), and the reference-stress solution (σ^r/σ_o) with the normalized distance from the crack-tip, $r\sigma_o/J_i$ at the load corresponding to the start of ductile tearing in each SENT specimen.

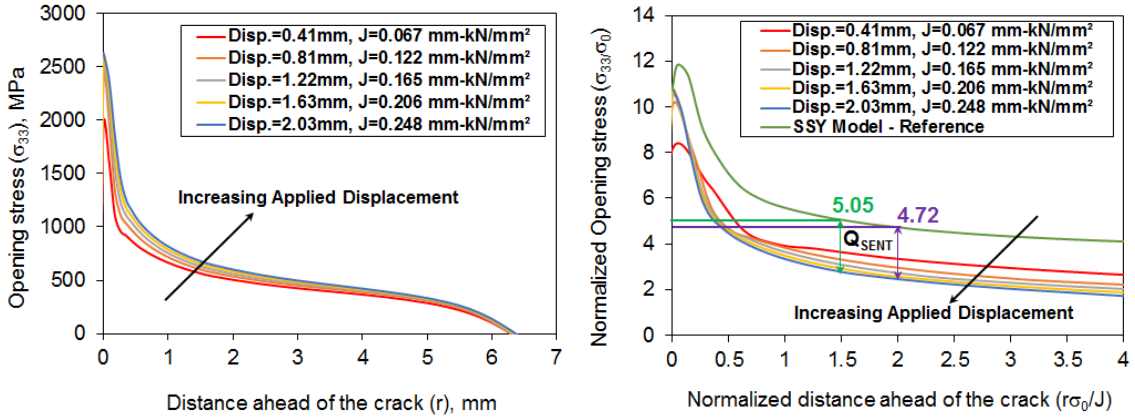

Figure 22. Opening mode stress, σ_{33}, with the increasing applied displacement up to the start of ductile tearing from the FEA of the SENT specimen with a_i/W=0.29; and normalized opening mode stress, σ_{33}/σ_o (for a/W=0.29 specimen), and the reference stress variation (σ^r/σ_o) with the normalized distance from the crack-tip, $r\sigma_o/J$ up to the start of ductile tearing.

Table 1. Change in $J_{applied}$ and Q at $r\sigma_o/J=1.5$ and 2 with loading (applied remote-displacement on the SENT specimen with $a_i/W=0.29$) up to the start of ductile tearing.

Displacement, mm	J, mm-kN/mm^2	Q at $r\sigma_o/J=1.5$	Q_i at $r\sigma_o/J=2.0$
0	0	0	0
0.41	0.067	-1.456	-1.421
0.81	0.122	-1.810	-1.839
1.22	0.165	-2.028	-2.062
1.63	0.206	-2.194	-2.206
2.03	0.248*	-2.330	-2.311

* Initiation toughness condition

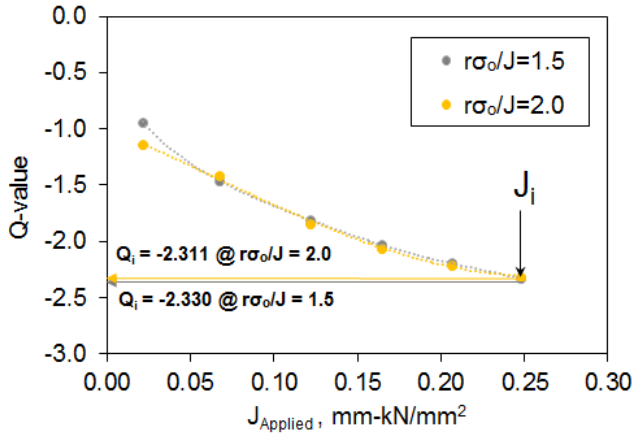

Figure 23. Variation of Q with applied J examined at distances of $r\sigma_o/J = 1.5$ and 2 from FEA of shallow-cracked SENT specimen with $a_i/W=0.29$.

DISCUSSION AND CONCLUSIONS

The following observations were made from the experimental investigations of SENT, CT, and circumferential/axial surface-cracked pipes and FEA investigations of the SENT specimens with three different crack depths. The opening-mode stress, plastic zone, and development of constraint at the start of ductile tearing (crack-initiation) were analyzed to drawn specific conclusions.

- Toughness values from a C(T) specimen are not always conservative! The initiation toughness determined for a few cases presented in this investigation revealed that the initiation toughness of a surface-crack with a/t~0.7 was roughly 40% of the C(T) crack-initiation toughness. Additional evaluations are needed to establish any trends for various materials.
- Relationship between CT and SENT specimen crack-initiation toughness depends on constraint as well as elastic-plastic material response, such as function of strain-hardening parameters and is an area of ongoing research.
- Past work on semi-empirical relationships connecting the axial surface-cracked pipe behavior to SENT or CT, Charpy specimen toughness have now been shown to have implicitly included the effects of toughness change with flaw depth as well as the effects of bulging factors. A commonly employed surface flaw bulging factor, $M_p = [1-a/(tM_T)]/(1-a/t)$ for axial surface-cracked pipes

potentially includes the effect of toughness change with flaw depth and pipe bulging effects (M_T is the Folias through-wall-crack bulging factor).

- Numerical/analytical determinations have included toughness values that are constant (obtained from CT or SENT, or adapted from Charpy tests) and compared to crack driving forces to determine ductile tearing. It is evident from the experimental and FEA investigations discussed here that there is need to account for toughness changes with surface crack depth exhibited by the material response, failing which the fracture predictions could be very conservative for deeper surface cracks. This was seen in all materials investigated in this work over a range of yield and ultimate stress values.
- Evaluation of the SENT and circumferential SC-Pipe test results for TP304 showed crack-initiation fracture toughness (J_i) differences between the two geometries that were an order of 3 ~ 4 larger in the SC-Pipe compared to the SENT specimens with the same normalized initial crack depth (a_i/t,a_i/W). Similarly, the fracture toughness parameter, CTOD at crack-initiation was found to be between 6 ~7 times higher in the SC-Pipe when compared to the SENT specimen with the same normalized crack depth. These results are under additional evaluations as they are different from commonly seen trends of SENT initiation toughness being close to SC-Pipe.
- The FEA results clearly showed that the constraint parameter, Q at the start of ductile tearing in the SENT specimens (denoted by Q_i) was roughly the same over a normalized distance of $0.25J_i/\sigma_o$ to $1.5J_i/\sigma_o$ rather than the commonly employed location of $2J_i/\sigma_o$ in constraint evaluation studies. The results were promising in nature, since one SENT test result (single a_i/W) could be used to obtain the fracture initiation toughness, J_i value for any other shallower or deeper SENT specimen with a different a_i/W. Additionally, the toughness trend observed was consistent with all the experimental trends investigated here for several materials.

ACKNOWLEDGEMENTS

The authors would like to acknowledge the support of Emc^2 staff members (Mr. Russell Hattery, Mr. Michael Fishman, Mr. George Wall, Mr. Paul Mincer), who were involved in the experimental work. The authors would also like to acknowledge the technical discussions with Dr. Robert Dodds, Jr. on the small-scale-yielding (SSY) model reference solution and providing WARP3D SSY model for the FE analysis.

REFERENCES

Anderson, T. L. (2014). "Assessment of Seam Weld Cracks: Technology Advances and Myth Busters", *DOT R&D Forum*.

ASME Section XI, Boiler and Pressure Vessel Code, 2016 Edition, Appendix C.

ABAQUS, Finite Element Analysis Software, Simulia, Dassault Systemes.

Dodds, R.H. (1994). "Constraint Effects on Fracture Initiation Loads in HSST Wide-plate Tests," NUREG/CR-6259.

Eiber, R. J., W. A. Maxey, W. A., Duffy, A. R. (1971). "Investigation of the Initiation and Extent of Ductile Pipe Rupture", *Battelle Memorial Institute Report, BMI-1908*.

Graba, M. (2008). "The Influence of Material Properties on the Q-Stress Value Near the Crack Tip for Elastic-Plastic Materials," *J. Theo. Appl. Mech.*, 46, 2, pp. 269-290.

Hackett, E.M., Schwalbe, K.H., Dodds, R.H. (1991). "Constraint Effects in Fracture", *ASTM STP-1171, Indianapolis*, May 8-9.

Hioe, Y., Kalyanam, S., Wilkowski, G., Pothana, S., Martin, J. (2017). "Fracture Toughness Variation with Flaw Depth in Various Specimen Geometries and Role of Constraint in Material Fracture Resistance," *PVP2017-65441, Proc. ASME Pressure Vessels & Piping Conf., Hawaii, July 16-20.*

Hutchinson, J.W. (1968). "Singular Behaviour at the End of a Tensile Crack in a Hardening Material" *J. Mech. Phys. Solids*, 16 (1), pp. 13–31.

Kalyanam, S., Beaudoin, A., Dodds, R.H., Barlat, F. (2009). "Delamination Cracking in Advanced Aluminum-Lithium Alloys – Experimental and Computational Studies", *Engg. Frac. Mech.*, 76, 14, pp. 2174-2191.

Kalyanam, S., Wilkowski, G.M., *et al.* (2010). "Why Conduct SEN(T) Tests and Considerations in Analyzing Testing SEN(T) Testing," *IPC2010-31631, 8th Intl. Pipeline Conf.*, Calgary, Canada.

Kalyanam, S., Wilkowski, G. M., *et al.* (2017). "Apparent Net-Section Collapse Methodology for Circumferential Surface Flaws in Piping," *PVP2017-65438, Proceedings of the ASME Pressure Vessels and Piping Conference, Hawaii, July 16-20.*

Kalyanam, S., Wilkowski, G.M., et al. (2019). "Constraint Effects When Determining Fracture Toughness/Material Fracture Resistance from Surface Cracked Elbows, CT, and SENT Specimens", SMiRT25, Aug 4 – 9. Charlotte, North Carolina, USA.

McMeeking, R.M., Parks, D.M. (1979). "On Criteria for J-Dominance of Crack Tip Fields in Large-Scale Yielding," *ASTM STP 668*, American Society for Testing and Materials, pp. 175-194.

Larossa, N.O., R. A. Ainsworth, R.A. (2016). "Ductile Fracture Modeling and J-Q Fracture Mechanics: A Constraint-Based Fracture Assessment Approach," *Frattura ed Integrita Strutturale*, 38, pp.266-272.

Maxey, W.A., and others (1972). "Ductile Fracture Initiation, Propagation, and Arrest in Cylindrical Vessels", *Fracture Toughness, Proceedings of the 1971 National Symposium on Fracture Mechanics, Part II*, ASTM STP 514, American Society for Testing and Materials, pp. 70 – 81.

O'Dowd, N.P. (1995). "Applications of Two Parameter Approaches in Elastic-Plastic Fracture Mechanics", *Engg. Frac. Mech.*, 52, 3, pp.445-465.

O'Dowd, N.P., Shih, C.F. (1991). "Family of Crack-Tip Fields Characterized by a Triaxiality Parameter – I, Structure of Fields," *J. Mech. Phys. Solids*, Volume 39, Issue 8, pp. 989-1015.

O'Dowd, N.P., Shih, C.F. (1991). "Family of Crack-Tip Fields Characterized by a Triaxiality Parameter – II, Fracture Applications," *J. Mech. Phys. Solids*, Volume 40, Issue 5, pp. 939-963.

O'Dowd, N.P., Shih, C.F., Dodds, R.H. (1995) "The Role of Geometry and Crack Growth on Constraint and Implications for Ductile/Brittle Fracture", *Constraint Effects in Fracture Theory and Applications: Second Volume, ASTM STP 1244*, M. Kirk, A. Bakker, Philadelphia.

Park, D.Y., (2010). "Evaluation of Fracture Toughness of X100 Pipe Steel Using SEN(B) and Clamped SE(T) Single specimens", *IPC2010-31282, 8th Intl. Pipeline Conf.*, Calgary, Canada.

Rice, J.R. (1968). "A Path Independent Integral and the Approximate Analysis of Strain Concentration by Notches Cracks", *J. Appl. Mech.*, 35, pp. 379-386.

Rice, J.R., Rosengren, G.F. (1968). "Plane Strain Deformation Near a Crack in a Power Law Hardening Material", *J. Mech. Phys. Solids*, 16, pp. 1-12.

Roychowdhury, S., Dodds, R.H. (2003). "A Numerical Investigation of 3-D Small-Scale Yielding Fatigue Crack Growth," *Engg. Frac. Mech*., 70 (17), pp. 2363-2383.

Roychowdhury, S., Dodds, R.H. (2005). "Modeling of Three-Dimensional Effects on Fatigue Crack Closure Processes in Small-Scale Yielding," *Fat. Frac. Mech. Matl.*, ASTM International, pp. 34.

Shim, D.J., Wilkowski, G.M., Brust, F., Horsley, D., Toch, M. (2010). "Applicability of Existing Fracture Initiation Models to High-Strength Steel Line Pipe," *Proc. 8th Intl. Pipeline Conf*., Calgary, Canada

Sobotka, J.C., Dodds, R.H. (2011). "Steady Crack Growth in a Thin, Ductile Plate Under Small-Scale Yielding Conditions: Three-dimensional Modeling", *Engg. Frac. Mech.*, 78, 2, pp. 343-363.

Stadtmüller, W., Sturm, D. (1995). "Leak-Before Break Behaviour of Austenitic and Ferritic Pipes Containing Circumferential Defects," in *LBB95 – Specialist Meeting on Leak-Before-Break in Reactor Piping and Vessels*, NUREG/CP-0155.

WARP3D, Open Source Code for 3D Nonlinear Analysis of Solids, Version 17.5.5, 2014.

Wilkowski, G.M., Eiber, R.J. (1981). "Evaluation of Tensile Failure of Girth Weld Repair Grooves in Pipe Subjected to Offshore Laying Stresses," *ASME Journal of Energy Technology*, pp. 48-57.

Wilkowski, G.M., Maxey, W.A. (1981). "Applications of the Electric Potential Method for Measuring Crack Growth in Specimens, Flawed Pipes, and Pressure Vessels," *ASTM 14th National Symposium on Fracture Mechanics*, Los Angeles, California, ASTM STP 791.